Journal of Pharmaceutical Analysis 14 (2024) 389–400

Contents lists available at ScienceDirect

Journal of Pharmaceutical Analysis

journal homepage: www.elsevier.com/locate/jpa

Original article

Antibody-platinum (IV) prodrugs conjugates for targeted treatment of cutaneous squamous cell carcinoma

Xiangye Yin [a,1], Yingjie Zhuang [a,1], Haiqin Song [b,1], Yujian Xu [a], Fan Zhang [a], Jianxin Cui [a], Lei Zhao [a], Yingjie Yu [c], Qixu Zhang [d], Jun Ye [e,***], Youbai Chen [a,**], Yan Han [a,*]

[a] Department of Plastic and Reconstructive Surgery, The First Medical Center, Chinese PLA General Hospital, Beijing, 100853, China
[b] Department of General Surgery, Ruijin Hospital, Shanghai Jiao Tong University School of Medicine, Shanghai, 200023, China
[c] State Key Laboratory of Organic-Inorganic Composites, Beijing Laboratory of Biomedical Materials, Beijing University of Chemical Technology, Beijing, 100029, China
[d] Department of Plastic Surgery, University of Texas MD Anderson Cancer Center, Houston, TX, 77030, USA
[e] State Key Laboratory of Bioactive Substance and Function of Natural Medicines, Institute of Materia Medica, Chinese Academy of Medical Sciences & Peking Union Medical College, Beijing, 100050, China

ARTICLE INFO

Article history:
Received 5 August 2023
Received in revised form
7 October 2023
Accepted 1 November 2023
Available online 4 November 2023

Keywords:
Antibody drug conjugate
Cutaneous squamous cell carcinoma
DNA damage
Platinum drug
Targeted therapy

ABSTRACT

Antibody-drug conjugates (ADCs) are a new type of targeting antibodies that conjugate with highly toxic anticancer drugs via chemical linkers to exert high specificity and efficient killing of tumor cells, thereby attracting considerable attention in precise oncology therapy. Cetuximab (Cet) is a typical antibody that offers the benefits of good targeting and safety for individuals with advanced and inoperable cutaneous squamous cell carcinoma (cSCC); however, its anti-tumor activity is limited to a single use. Cisplatin (CisPt) shows good curative effects; however, its adverse effects and non-tumor-targeting ability are major drawbacks. In this study, we designed and developed a new ADC based on a new cytotoxic platinum (IV) prodrug (C8Pt(IV)) and Cet. The so-called antibody-platinum (IV) prodrugs conjugates, named Cet-C8Pt(IV), showed excellent tumor targeting in cSCC. Specifically, it accurately delivered C8Pt(IV) into tumor cells to exert the combined anti-tumor effect of Cet and CisPt. Herein, metabolomic analysis showed that Cet-C8Pt(IV) promoted cellular apoptosis and increased DNA damage in cSCC cells by affecting the vitamin B6 metabolic pathway in tumor cells, thereby further enhancing the tumor-killing ability and providing a new strategy for clinical cancer treatment using antibody-platinum (IV) prodrugs conjugates.

1. Introduction

A typical antibody-drug conjugate (ADC) comprises a monoclonal antibody linked to a cytotoxic drug via chemical linkers to specifically deliver the toxic payload to specific tumor cells [1–4]. The high specificity and effectiveness of ADCs, with minimal damage and toxicity to normal tissues, make them highly desirable for cancer therapy. The major advantage of ADCs over traditional chemotherapeutic drugs is their wide therapeutic window [5,6]. However, ADCs also have some defects. First, ADCs comprises cytotoxic medications connected to therapeutic monoclonal antibodies through chemical bonds, and current linkers are generally undesirable because of the difficulty in their chemical design with tedious synthetic steps and high costs [7–10]. Second, apart from ultra-high cytotoxicity, the current cytotoxic drugs carried by ADCs mostly have a narrow therapeutic anticancer spectrum or limited anticancer activity, displaying activity against only a single cancer type or a small number of cancer types, and they are inefficient in killing cancer cells by themselves [11–13]. Therefore, future development of ADCs may focus on reducing costs by simplifying the linker design and extending ADCs for broader therapeutic applications.

The platinum compound is one of the most commonly used classes of antineoplastic drugs in clinics, with a broad anticancer spectrum for malignant tumors, such as lung cancer, colorectal cancer, ovarian cancer, and head and neck squamous cell carcinoma

Peer review under responsibility of Xi'an Jiaotong University.
* Corresponding author.
** Corresponding author.
*** Corresponding author.
E-mail addresses: yejun@imm.pumc.edu.cn (J. Ye), chenyoubai@301hospital.com.cn (Y. Chen), 13720086335@163.com (Y. Han).
[1] These authors contributed equally to this work.

https://doi.org/10.1016/j.jpha.2023.11.002

[14,15]. Research has indicated that cisplatin (CisPt)-based combination chemotherapy is a commonly used medication for cutaneous squamous cell carcinoma (cSCC), exhibiting an impressive overall response rate of up to 80% [16]. Although the combination chemotherapy regimen demonstrates remarkable effectiveness in treating inoperable or advanced cSCC, platinum-based drugs have serious systemic side effects owing to the lack of cancer targeting, resulting in difficulty in their accumulation at tumor sites [17]. Platinum (IV) drugs currently under study differ from traditional platinum (II) drugs, such as CisPt, owing to their fewer toxic adverse effects [18,19]. Platinum (IV) prodrugs have highly stable spatial octahedral structures and are kinetically inert, which are their basic characteristics. The lower propensity of platinum (IV) prodrugs to interact with biomolecules, such as serum proteins, limits their side effects; therefore, platinum (IV) drugs have lower systemic toxicity than traditional platinum (II) drugs [20]. After entering the highly reductive environment of tumors, platinum (IV) drugs are quickly reduced to their platinum (II) counterparts, which can exert DNA damaging effects [21–25]. However, platinum (IV) drugs lack tumor targeting ability, necessitating the use of drug delivery systems to achieve excellent anti-tumor effects [26,27].

Cetuximab (Cet) is a monoclonal antibody of the chimeric immunoglobulin G1 type that has high specificity for the epidermal growth factor receptor (EGFR), possesses greater binding strength than with epidermal growth factor, and results in the blocking of ligand-induced EGFR phosphorylation [28,29]. In view of its good tumor-targeting ability and excellent safety profile, Cet has been employed in the therapy of various solid tumors that exhibit high levels of EGFR expression, such as colorectal cancer, head and neck squamous cell carcinoma, and cSCC, among others [30–32]. Moreover, Cet-based monotherapy is well tolerated by elderly patients with advanced cSCC [16]. Therefore, it is more desirable to combine Cet with CisPt to achieve better therapeutic effects, owing to the limited anti-tumor activity of Cet and the side effects of CisPt in single-agent therapies for cSCC.

In this study, a new platinum (IV) prodrug, C8Pt(IV), was designed based on CisPt with broad-spectrum antineoplastic activity. Subsequently, a new ADC, namely Cet-C8Pt(IV), was developed by conjugating Cet with C8Pt(IV) via amide bonds by 1-ethyl-3-(3-dimethylaminopropyl)carbodiimide hydrochloride (EDCI) or *N*-hydroxy succinimide (NHS) chemistry [33–35]. The amide bonds were used as linkers of C8Pt(IV) and Cet via simple chemical conjugation to avoid the complicated linker design in a typical ADC (Scheme 1). In addition, Cet-C8Pt(IV) was found to have a better tumor-killing ability than CisPt. Furthermore, metabolomic analysis has shown that Cet-C8Pt(IV) promotes cancer cell apoptosis by inducing greater DNA damage in human skin squamous cell carcinoma A-431 cells [36]. Therefore, Cet-C8Pt(IV) has shown better targeting ability in both A-431 cells and in an orthotopic cSCC mouse model with high EGFR expression. This study paves the way for the development of therapeutic options for cSCC using antibody-platinum (IV) prodrugs conjugates.

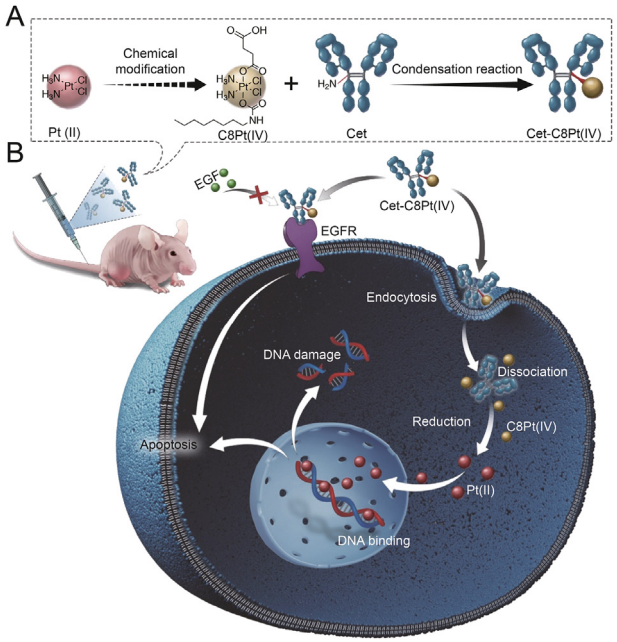

Scheme 1. Schematic illustration of preparation of antibody-platinum (IV) prodrugs conjugates of cetuximab (Cet)-C8Pt(IV) and possible anti-tumor mechanism of action. (A) Preparation of Cet-C8Pt(IV) via a condensation reaction of Cet with C8Pt(IV). (B) Possible mechanism of action of Cet-C8Pt(IV). Cet-C8Pt(IV) was injected into mice bearing A431 tumors and accumulated in cutaneous squamous cell carcinoma (cSCC) tumor tissues via tumor targeting. Cet-C8Pt(IV) exerted the anti-tumor effect by causing DNA damage in tumors cells and inducing tumor cell apoptosis. EGF: epidermal growth factor; EGFR: epidermal growth factor receptor.

2. Materials and methods

2.1. Reagents and chemicals

Cet was obtained from Merck KGaA (Darmstadt, Germany). CisPt was obtained from Boyuan Chemical Company (Shandong, China). Succinic anhydride (SA), 1-isocyanatooctane (C8-NCO), acetone, hydrogen peroxide, ether, *N*,*N*-dimethylformamide (DMF), dimethyl sulfoxide (DMSO), EDCI, and NHS were obtained from Aladdin (Shanghai, China). Unless otherwise specified, all chemicals were acquired from commercial suppliers and utilized without additional purification. The cell culture vessels were obtained from Corning Inc. (Corning, NY, USA). Dulbecco's modified Eagle's medium (DMEM) containing 4.5 g of glucose, Roswell Park Memorial Institute-1640 (RPMI-1640), trypsin-ethylenediamine tetraacetic acid (EDTA) (0.25%), penicillin/streptomycin, and fetal bovine serum were procured from Gibco (Grand Island, NY, USA). 4',6-diamidino-2-phenylindole (DAPI), propidium iodide (PI), Alexa Fluor® 488, and the terminal deoxynucleotidyl transferase dUTP nick-end labeling (TUNEL) apoptosis assay kit were acquired from Solarbio Science & Technology Co., Ltd. (Beijing, China). More detailed information about materials and method are shown in the Supplementary data.

2.2. Cell lines and animals

All the cells were supplied by the American Type Culture Collection (ATCC; Manassas, VA, USA). Beijing Vital River Laboratory Animal Technology Co., Ltd. (Beijing, China) provided healthy Kunming (KM) and BALB/c nude mice, which were raised in specific pathogen-free animal rooms. The animal experiments conducted in this study were carried out in accordance with the guidelines reviewed and approved by the Laboratory Animal Center of the Chinese PLA General Hospital, Beijing, China (Approval No.: 2021-X17-21).

2.3. Synthesis of C8Pt(IV)

CisPt (500 mg, 1.65 mmol) was dissolved in H_2O_2 (30% (*m*/*V*), 20 mL). The mixture was stirred at 40 °C overnight to a clear solution. After cooling to room temperature, numerous needle-like crystals were precipitated. The product, Pt(IV)-OH, was washed

several times with acetone and dried in a desiccator. Subsequently, Pt(IV)-OH (334 mg, 1 mmol) and succinic anhydride (100 mg, 1 mmol) were suspended in DMF (100 mL), and the mixture was stirred at 50 °C for 24 h to a clear solution. The DMF was then removed by rotary evaporation, the product (Pt(IV)-COOH) was washed several times with acetone and ether, and the precipitate was dried in a desiccator. Finally, Pt(IV)-COOH (434 mg, 1 mmol) and C8-NCO (170 mg, 1.1 mmol) were suspended in DMF (30 mL), then the mixture was stirred at 55 °C for 12 h to a clear solution. Finally, the DMF was removed by rotary evaporation, the product (C8Pt(IV)) was washed several times with acetone and ether, and the precipitate was dried in a desiccator.

2.4. Synthesis of Cet-C8Pt(IV)

EDCI (1.6 mg) and NHS (1 mg) was added to a solution of C8Pt(IV) (5 mg) in DMSO (200 μL). The mixture was incubated for 30 min at room temperature. The reaction mixture was added dropwise to Cet in water (1.25 mg/mL, 40 mL). Next, the reaction mixture was stirred for 8 h at room temperature. Then, the solution was subsequently purified with Vivaspin 6 (three times, molecular weight cut-off (MWCO) 30 kDa) to remove unconjugated C8Pt(IV). Finally, Cet-C8Pt(IV) was prepared and stored until further use.

2.5. Pt release of Cet-C8Pt(IV)

A volume of 5 mL of Cet-C8Pt(IV) with a platinum concentration of 100 μM was moved into a dialysis bag (MWCO: 3.5 kDa) that had been pre-swelled. The bag was subsequently placed in either 200 mL of phosphate-buffered saline (PBS) or sodium ascorbate (NaVc) (200 mL, 10 mM NaVc) in a shaking culture incubator set at 37 °C. At different time intervals, 1 mL of the solution was extracted, and an equivalent amount of a new solution was promptly introduced into the incubation medium following the sampling process. The platinum concentrations were measured by inductively coupled plasma mass spectrometry (ICP-MS; Agilent Technologies 7,700 series; Santa Clara, CA, USA).

2.6. Cell uptake of Cet-C8Pt(IV)

A confocal laser scanning microscope (CLSM; LSM-800, ZEISS, Oberkochen, Germany) was used to monitor the cellular absorption of Cet-C8Pt(IV). Briefly, a cover glass was inserted into each well of a 24-well plate. A volume of 1 mL of media at a total of 1×10^5 A-431 cells was added into each well and incubated at 37 °C for 12 h. Next, cells were exposed to Cet-C8Pt(IV)@Cy5.5 (5 μM Pt) for 0, 0.5, 3, or 6 h. Cells were fixed in paraformaldehyde and washed with cold PBS. DAPI was used to stain the nuclei. The cytoskeletons were stained with actin (Beyotime Biotechnology Co., Ltd., Shanghai, China). Subsequently, images were collected with CLSM (DAPI: $\lambda_{ex} = 405$ nm and $\lambda_{em} = 460$ nm; Cy5.5: $\lambda_{ex} = 673$ nm and $\lambda_{em} = 692$ nm).

Flow cytometry was performed to examine the cellular internalization of Cet-C8Pt(IV). A-431 cells were seeded in 12-well plates at a density of 3×10^5 cells/well and incubated for 12 h. The cells were then exposed to Cet-C8Pt(IV)@Cy5.5 for 0, 0.5, 3, or 6 h, rinsed with PBS, and analyzed using flow cytometry (FCM; Beckman Coulter, Brea, CA, USA).

2.7. Cell viability assays

A-431 cells were placed in 96-well plates with a density of 5×10^3 cells/well and incubated for 12 h. Subsequently, the cells were exposed to PBS, CisPt, Cet, CisPt + Cet, C8Pt(IV), C8Pt(IV) + Cet, or Cet-C8Pt(IV) at varying concentrations from 0.000625 to 5 μM for platinum for a duration of 48 h. The Cet concentration ranged from 0.015 to 120 μg/mL in the Cet, CisPt + Cet, and C8Pt(IV) + Cet groups. The cells were subsequently cultured in a 10% 3-(4, 5-dimethylthiazol-2-yl)-2,5-diphenyltetrazolium bromide (MTT) solution for a duration of 4 h, followed by measurement at a wavelength of 570 nm. After 12 h, 100 μL of sodium dodecyl sulfate (SDS) were introduced into each well of the 96-well plates. Subsequently, absorbance was determined using microplate reader (SpectraMax M8; Molecular Devices, San Jose, CA, USA).

2.8. Apoptosis analysis

Cell apoptosis was evaluated using the annexin V-fluorescein isothiocyanate (FITC) apoptosis detection kit (Elabscience Biotechnology Co., Ltd., Wuhan, China), according to the manufacturer's guidelines. Briefly, A-431 cells were seeded into 12-well plates at a density of 3×10^5 cells/well. Following a 12-h incubation period, the cells were exposed to PBS, CisPt, Cet, CisPt + Cet, C8Pt(IV), C8Pt(IV) + Cet, or Cet-C8Pt(IV) (platinum at 5 μM and Cet at 120 μg/mL) for 24 h. Subsequently, the cells were rinsed with PBS and subjected to a 15-min incubation with annexin/PI reagent in a dark environment at 37 °C. Thereafter, FCM was used to promptly measure the cells.

2.9. Western blot analysis

Radioimmune precipitation assay (RIPA) lysis buffer (P0013B, Beyotime) was used to treat A-431 cells. Proteins from A-431 cells were obtained by centrifugation at 12,000 r/min for 15 min. The protein concentration was determined using a bicinchoninic acid (BCA) assay (P0011, Beyotime). Equal quantities of proteins were separated by SDS-polyacrylamide gel electrophoresis (PAGE) and transferred onto polyvinylidene fluoride (PVDF) membranes. After that, the membranes were blocked in Tris-buffered saline with Tween 20 (TBS-T) with 5% non-fat milk for 1 h. Next, the membranes were placed on a shaker at 4 °C overnight and incubated with a primary antibody against EGFR (GB111504; Servicebio Technology Co., Ltd., Wuhan, China). The PVDF films were then washed three times for 30 min each time. The cells were then incubated with horseradish peroxidase (HRP)-conjugated antibodies (A0208, Beyotime) at room temperature for 2 h. A gel imaging system (Tanon 4800, Shanghai, China) was used to acquire Western blot images. Glyceraldehyde-3-phosphate dehydrogenase (GAPDH) (#5174; Cell Signaling Technology, Boston, MA, USA) was used as a control for protein loading.

2.10. Metabolomics

Cells were cultivated in triplicate in the 6-well plates and respectively treated with PBS, CisPt, C8Pt (IV), and Cet-C8Pt(IV) at a concentration of 2.5 μM of platinum for 24 h. Next, the cells were washed twice with 1× PBS and subsequently extracted using 500 μL of ice-cold extraction solvent (water:methanol:chloroform (100:180:120, *V*/*V*/*V*)). Following a thorough shaking for a duration of 1 min, the Eppendorf tube was loaded with a combined volume of 150 μL water and subsequently subjected to centrifugation at 1,000 *g* for 15 min at 4 °C. For metabolomic analysis, 400 μL of the supernatant was moved into vials for liquid chromatography (LC) (Thermo Fisher Scientific Inc., San Jose, CA, USA), then subjected to centrifugation to remove moisture, and finally reconstituted to a final volume of 40 μL. Ultra high-performance liquid chromatography (UHPLC)-electron spray ionization (ESI)-orbitrap-MS (Thermo Fisher Scientific Inc.) successfully identified all the

metabolites. A compound discoverer (version 3.1) was used to identify and quantify the data. MetaboAnalyst 5.0 (https://www.metaboanalyst.ca/) was used for metabolic data statistics and enrichment analysis.

2.11. In vivo biodistribution of Cet-C8Pt(IV)

To generate mice with solid tumors of either 4T1 or A-431 cells, BALB/c-nu mice were injected with 5×10^6 4T1 or A-431 cells subcutaneously in the right hip. Upon the tumor reaching approximately 200 mm^3 in size, mice with 4T1 tumors were administered an intravenous injection of Cet@Cy5.5 at a dosage of 1 mg/kg. Upon reaching approximately 200 mm^3 of tumor volume, mice bearing A-431 tumors were intravenously injected with either Cet@Cy5.5 (1 mg/kg) or Cet-C8Pt(IV)@Cy5.5 (1 mg/kg). Subsequently, imaging was performed using Impact of Visual Impairment after Stroke (IVIS) spectrum (PerkinElmer, Waltham, MA, USA) at 3, 6, 8, 12, 24, and 36 h after injection (excitation, 675 nm; emission, 720 nm). The mice were sacrificed 36 h after injection, and the tumors and specific organs were extracted and imaged.

2.12. In vivo antitumor efficacy evaluation

On days 0, 3, and 6, five groups of mice with A-431 tumors were randomly selected. These groups were then randomly administered intravenous injections of PBS, Cet, CisPt, CisPt + Cet, or Cet-C8Pt(IV) (3 mg/kg platinum or 10 mg/kg Cet). The tumor sizes and weights in each group were measured every other day, and the tumor size (V, mm^3) was determined using the formula: $V = (a \times b^2)/2$, where a represents the length of the tumor and b represents its width.

2.13. Statistical analysis

Data were displayed as the mean ± standard deviation (SD). Graphpad Prism 8 was used to analyze the data. Student's t-test and one-way analysis of variance (ANOVA) were performed. Statistical significance was determined at a significance level of $^{*}P < 0.05$, $^{**}P < 0.01$, and $^{***}P < 0.001$.

3. Results and discussion

3.1. Expression of EGFR in patient samples, cell lines, and mouse models

To explore the ability of Cet to target skin squamous cell carcinoma, bioinformatics analysis of the GSE98767 data-set in the Gene Expression Omnibus (GEO) database was conducted. The GSE98767 dataset is a high-throughput sequencing dataset comprising 54 samples, including 9 samples from normal human keratinized epithelial tissues and 45 samples from human skin squamous cell carcinoma tissues. The limma package of R was used to examine the differences between normal human keratinized epithelial tissues and human skin squamous cell carcinoma tissues. First, EGFR was significantly overexpressed in cSCC (Fig. 1A). Next, the expression of EGFR was compared between tumor and normal keratinized epithelial tissues. High expression of EGFR was evident in cSCC tumors, with a significantly higher level than that in normal human keratinized epithelial tissues (log2(fold change) = 2.729, $P < 0.001$) (Fig. 1B). To verify the above bioinformatics analysis results, tumor and adjacent normal tissues from patients with cSCC were subjected to hematoxylin and eosin (H&E) and immunohistochemical staining (Figs. 1C and D). These findings confirmed that tumor tissues exhibited significant overexpression of EGFR, whereas normal tissues did not. In addition, EGFR expression was detected in a cell line derived from human skin squamous cell carcinoma, namely A-431. Sixty-nine kinds of normal cell lines and cancerous cell lines were compared. The findings indicate that A-431 cells exhibit significantly elevated expression of EGFR, surpassing the levels observed in other cell lines (Fig. S1). Subsequently, EGFR expression in A-431 cells was measured by Western blotting. According to these findings, the level of EGFR expression in A-431 cells was significantly higher than that in the mouse breast cancer cell line 4T1 and the mouse squamous cell carcinoma cell line SCC-7 (Fig. 1E). Finally, an orthotopic cSCC tumor model in immunodeficient mice was established by subcutaneous injection of A-431 tumor cells [37,38]. Tumors, adjacent skin tissues, and muscle tissues were collected for immunofluorescence staining of EGFR (red) in the tumor-bearing mice (Figs. 1F and G). Once again, the findings demonstrated that EGFR was significantly expressed in the tumors of mice bearing orthotopic cSCC tumors. These results confirmed that EGFR was highly expressed in tumor tissues from patients with cSCC, A-431 cell lines, and tumor tissues of mice with orthotopic cSCC tumors, which is in accordance with the underlying premise of Cet therapy.

3.2. Preparation and characterization of Cet-C8Pt(IV)

To obtain Cet-C8Pt(IV), CisPt was oxidized to Pt(IV)-OH. Subsequently, succinic anhydride was used to functionalize Pt(IV)-OH, resulting in the formation of Pt(IV)-COOH with a single carboxyl substitution. Subsequently, Pt(IV)-COOH was linked to C8-NCO to obtain C8Pt(IV) (Fig. 2A). Finally, Cet-C8Pt(IV) was prepared via the condensation of the carboxyl groups on C8Pt(IV) and the amine groups on Cet (Fig. 2B). Next, C8Pt(IV) was characterized using nuclear magnetic resonance (NMR) (Figs. S2–S4), high performance liquid chromatography (HPLC), and high-resolution MS (Fig. S5). The drug-to-antibody ratio (DAR) is a key characteristic of ADC drugs and represents the average quantity of drugs conjugated to antibodies. DAR determines both the efficacy and clearance rate of ADC drugs, which typically ranges from 0 to 8, indicating that there were 0–8 conjugated molecules per antibody [39–41]. Compared with Cet (m/z = 152659.2), Cet-C8Pt(IV) displayed four major m/z peaks. These peaks could be attributed to Cet conjugated with different amounts of C8Pt(IV) (Figs. 2C and D). Furthermore, the ICP-MS analysis revealed that the average DAR was 6.1. The drug-release behavior of Cet-C8Pt(IV) was examined using ICP-MS under various conditions. The findings indicated that the release of platinum from Cet-C8Pt(IV) after 48 h of incubation in 10 mM of NaVc (HAA^-) was 4.9 times greater than that in PBS during the same period, indicating that Cet-C8Pt(IV) could release platinum efficiently in a highly reductive tumor environment in cancer cells (Fig. S6). In summary, the ADC drug Cet-C8Pt(IV) was designed with an ideal DAR that could efficiently release drugs into the tumor environment.

3.3. Anti-tumor activity of Cet-C8Pt(IV) in vitro

Intracellular uptake of Cet-C8Pt(IV) plays a role in its anticancer activity. First, the platinum concentration in the tumor cells was measured separately at 0.5, 3, and 6 h after treating the cells with C8Pt(IV), a combination of C8Pt(IV) and Cet and Cet-C8Pt(IV). According to these findings, tumor cells treated with Cet-C8Pt(IV) exhibited significantly elevated levels of platinum compared to cells subjected to alternative treatments. The platinum concentration in these cells was observed to be as high as 6.83 and 6.58 times greater than that of cells treated with C8Pt(IV) and a combination of C8Pt(IV) and Cet, respectively (Fig. 3A). Subsequently, tumor targeting of Cet-C8Pt(IV) by A-431 cells was confirmed via a competitive inhibition experiment. A-431 cells were pretreated

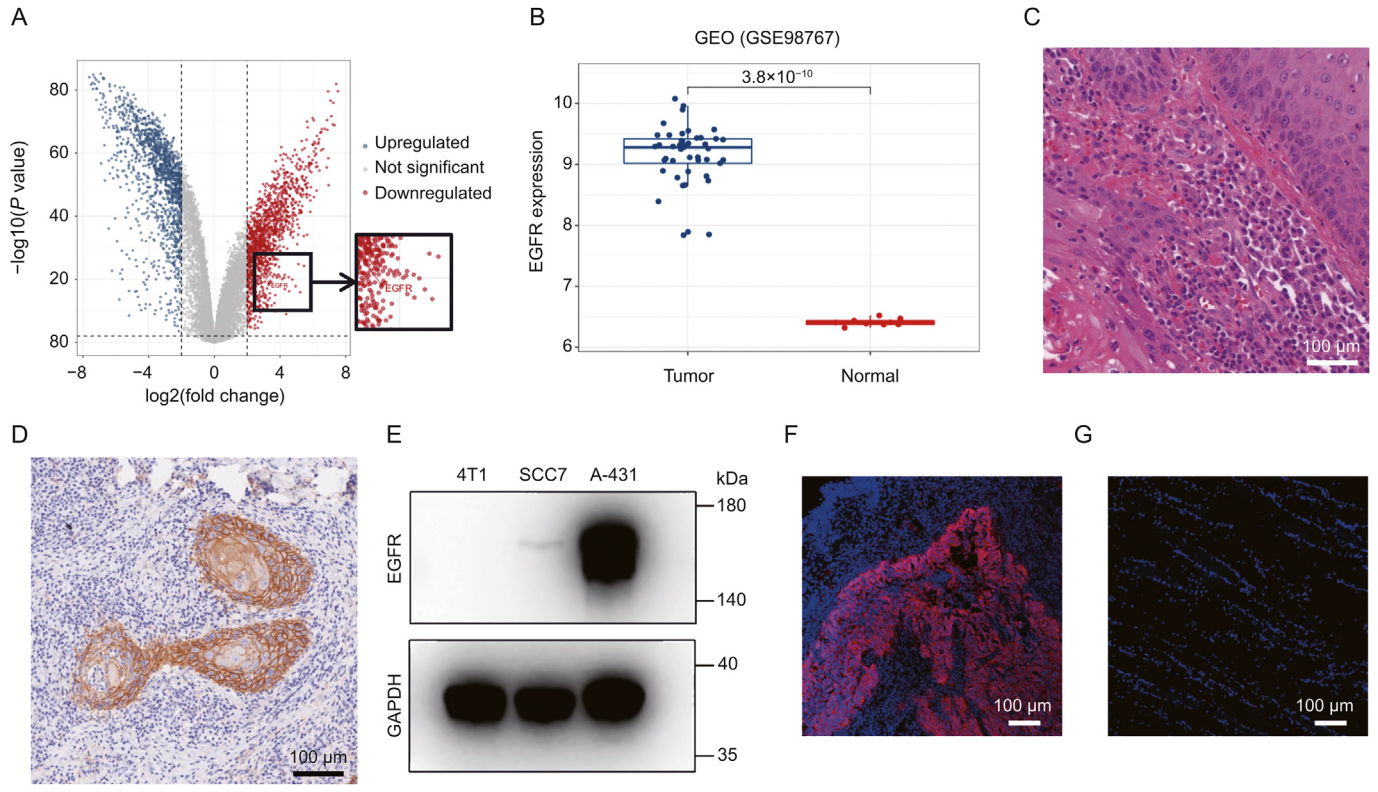

Fig. 1. The epidermal growth factor receptor (EGFR) was highly expressed in tumor tissues of cutaneous squamous cell carcinoma (cSCC) patients, A-431 cell line, and tumor tissues of orthotopic cSCC tumor mouse models. (A) Differential expression analysis of high-throughput sequencing data between normal human keratinized epithelial tissues and human skin squamous cell carcinoma tissues from GSE98767 data set in Gene Expression Omnibus (GEO) database. (B) Expression of EGFR in cSCC tumor tissues and human normal keratinized epithelial tissues. (C) Hematoxylin and eosin (H&E) staining of human cSCC tumor tissues. (D) Immunohistochemical staining of EGFR in human cSCC tumor tissues. (E) Expression of EGFR in different cell lines detected by Western blotting. (F, G) Immunofluorescence detection of EGFR expression in tumor (F) and adjacent muscle (G) tissues in orthotopic cSCC mouse models. GAPDH: glyceraldehyde-3-phosphate dehydrogenase.

with Cet and then treated with Cet-C8Pt(IV). The findings indicated that the concentration of platinum in A-431 cells that were not pretreated with Cet was 1.83 times greater compared to cells that underwent Cet pretreatment. This suggests that Cet-C8Pt(IV) effectively targets EGFR in tumor cells, demonstrating its potential for tumor eradication (Fig. 3B). Next, to measure the absorption of Cet-C8Pt(IV) by A-431 cells, Cet-C8Pt(IV) was tagged with the fluorescent dye Cy5.5 (Cet-C8Pt(IV)@Cy5.5), which was further incubated with A-431 cells for 0, 0.5, 3, and 6 h. According to the FCM findings, the fluorescence intensity of A-431 progressively increased with the treatment time of Cet-C8Pt(IV)@Cy5.5. Specifically, the A-431 cells exhibited a fluorescence intensity that was 3.1 and 1.9 times greater at 6 h compared to cells treated for 0.5 and 3 h, respectively (Figs. 3C and D). CLSM was used to visualize the absorption of Cet-C8Pt(IV)@Cy5.5 by A-431 cells. The intensity of red fluorescence in the A-431 cells treated with Cet-C8Pt(IV)@Cy5.5 increased with treatment time (Fig. 3E).

Subsequently, the antiproliferative activity of Cet-C8Pt(IV) was tested in cancer cells. The MTT assay of Cet-C8Pt(IV) in A-431 cells was performed. The results showed that CisPt at 5 μM had an inhibition rate of only approximately 27% of tumor cells in A-431 cells, whereas a combination of CisPt (5 μM) + Cet (120 μg/mL) had an inhibition rate of approximately 34% in A-431 cells. However, Cet-C8Pt(IV) at the same concentration had an inhibition rate at approximately 86% on A-431 cells, which was 2.5 times higher than that of CisPt (5 μM) + Cet (120 μg/mL) (Fig. 3F), indicating that Cet-C8Pt(IV) was an effective antitumor agent. Apoptosis of A-431 cells in the different treatment groups was assessed using annexin V-FITC/PI dual staining. According to the findings, Cet-C8Pt(IV) at 5 μM resulted in an apoptosis rate as high as 83.9%, whereas CisPt and C8Pt(IV) caused an apoptosis rate at 7.8% and 58.3%, respectively (Fig. 3G), indicating that Cet-C8Pt(IV) induced more apoptosis than CisPt and C8Pt(IV) at the same platinum concentration due to its compound selectivity caused by the antibody Cet-C8Pt(IV) conjugated with. These findings suggest that Cet-C8Pt(IV) may play a role in cancer cell apoptosis. Finally, colony formation experiments verified that Cet-C8Pt(IV) effectively suppressed colony formation by A-431 cells (Fig. 3H). In summary, Cet-C8Pt(IV) displayed the more efficient anticancer activity *in vitro*.

3.4. Metabolomic analysis of A-431 cells treated with Cet-C8Pt(IV)

To better understand the mechanism of Cet-C8Pt(IV) action, a metabolomic study of A-431 cells treated with various medications was performed using LC/MS. Initially, the heat map showed the metabolites of A-431 cells treated with PBS, CisPt, C8Pt(IV), and Cet-C8Pt(IV) (Fig. 4A). The results indicated a clear and notable distinction in the metabolites of A-431 when treated with PBS compared to that with the other three medications. Next, Kyoto Encyclopedia of Genes and Genomes (KEGG) enrichment analysis of the metabolites in A-431 cells treated with PBS and Cet-C8Pt(IV) was conducted. The findings indicated that the synthesis of pantothenate and CoA, metabolism of glycine, serine, and threonine, metabolism of vitamin B6, and metabolism of arginine and proline were notably enhanced in the metabolites of A-431 cells subjected to Cet-C8Pt(IV) treatment (Fig. 4B). Subsequently, KEGG enrichment analysis of the cell metabolites treated with other drugs was performed. The results indicated that the

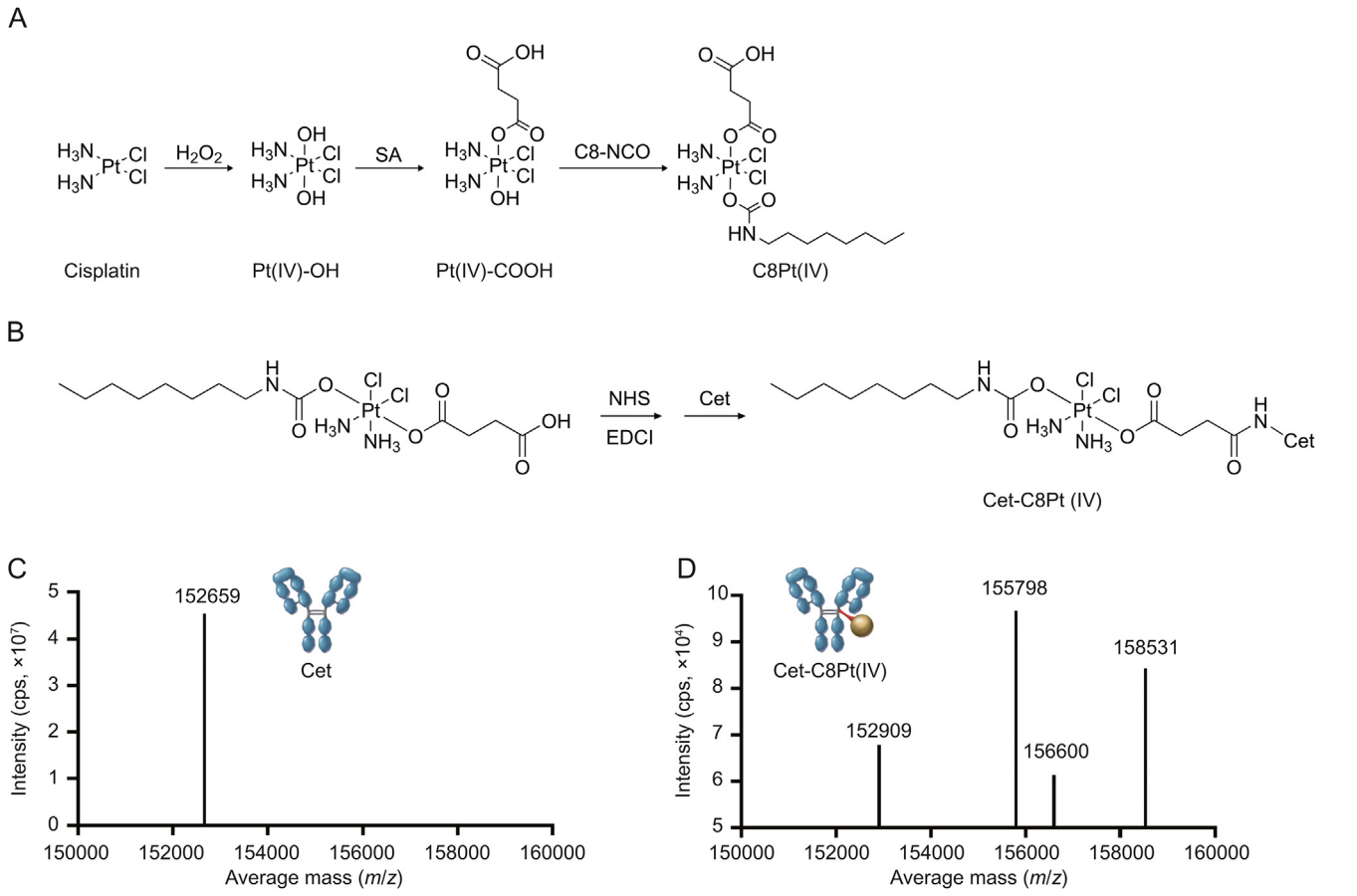

Fig. 2. Preparation and characterization of cetuximab (Cet)-C8Pt(IV). (A) The synthesis route of C8Pt(IV). (B) The synthesis route of Cet-C8Pt(IV). (C) High resolution electrospray ionization (ESI) of Cet. (D) High resolution ESI of Cet-C8Pt(IV). SA: Succinic anhydride; C8-NCO: 1-isocyanatooctane; EDCI: 1-ethyl-3-(3-dimethylaminopropyl)carbodiimide hydrochloride; NHS: *N*-hydroxy succinimide.

four most significantly enriched pathways for metabolites in CisPt-treated A-431 cells were primary bile acid biosynthesis, taurine and hypotaurine metabolism, aminoacyl-transfer RNA (tRNA) biosynthesis, and pantothenate and CoA biosynthesis (Fig. S7). However, the four most significantly enriched pathways for metabolites in A-431 cells treated with C8Pt(IV) were the lysine degradation, glycine, serine, and threonine metabolism, glycosylphosphatidylinositol (GPI)-anchor biosynthesis, and vitamin B6 metabolism (Fig. S8). Based on the integrated analysis of the metabolic pathways of cells with various treatments, Cet-C8Pt(IV) and C8Pt(IV) in A-431 cells act differently from traditional platinum drugs, such as CisPt. Subsequently, Pantothenate and CoA biosynthesis in cells exposed to Cet-C8Pt(IV) were found to be closely related to DNA damage and oxidative stress, which is likely one of the major pathways in cell killing [42–44]. However, it is worth noting that nephrotoxicity and ototoxicity induced by CisPt in patients are also associated with oxidative stress and a poor redox state balance. After entering tumor cells, platinum-based drugs can induce DNA damage via the formation of DNA cross-links, leading to the halting of the cell cycle and ultimately cell death [45–47]. In accordance with prior metabolomic studies, cells treated with Cet-C8Pt(IV) and C8Pt(IV) exhibited a notable enrichment in vitamin B6 metabolism. These results indicate that vitamin B6 could aggravate CisPt-mediated DNA damage by promoting the depletion of intracellular glutathione. Additionally, vitamin B6 can increase the sensitivity of tumor cells to apoptosis induced by various physical and chemical stresses, including chemotherapeutics, to enhance their tumor killing effects [36]. Furthermore, metabolomics was used to verify the DNA damage induced by Cet-C8Pt(IV). The DNA damage indicator γ-H2AX in the A-431 cells with various treatments were investigated using an immunofluorescence staining assay. The CLSM results indicated that the red fluorescence intensity in A-431 cells treated with Cet-C8Pt(IV) was notably greater than that in cells treated with C8Pt(IV) or a combination of C8Pt(IV) and Cet (Fig. 4C). In summary, we found via metabolomic analysis that Cet-C8Pt(IV) exerted its cytotoxicity mainly through oxidative stress and DNA damage.

3.5. Biosafety and biodistribution of Cet-C8Pt(IV) in vivo

Biosafety is a key parameter before a drug enters any clinic [48,49]. ADCs have good targeting performance and exert better cell killing effect than traditional cytotoxic drugs [1,50]. Herein, the biosafety of Cet-C8Pt(IV) was investigated in healthy KM mice. Briefly, the mice received different medications at a dose of 3 mg of Pt/kg based on body weight and 10 mg/kg Cet. Given its poor water solubility *in vivo*, C8Pt(IV) was excluded. Blood samples and organs were harvested after 15 days of treatment. Biochemical blood analysis showed almost no statistical difference between mice treated with Cet-C8Pt(IV) and PBS, indicating the negligible systemic toxicity of Cet-C8Pt(IV) (Fig. S9). In addition, examination of the major organs in mice treated with different therapies revealed no significant morphological alterations when comparing Cet-C8Pt(IV) to PBS, confirming the safety of Cet-C8Pt(IV) through H&E staining (Fig. S10).

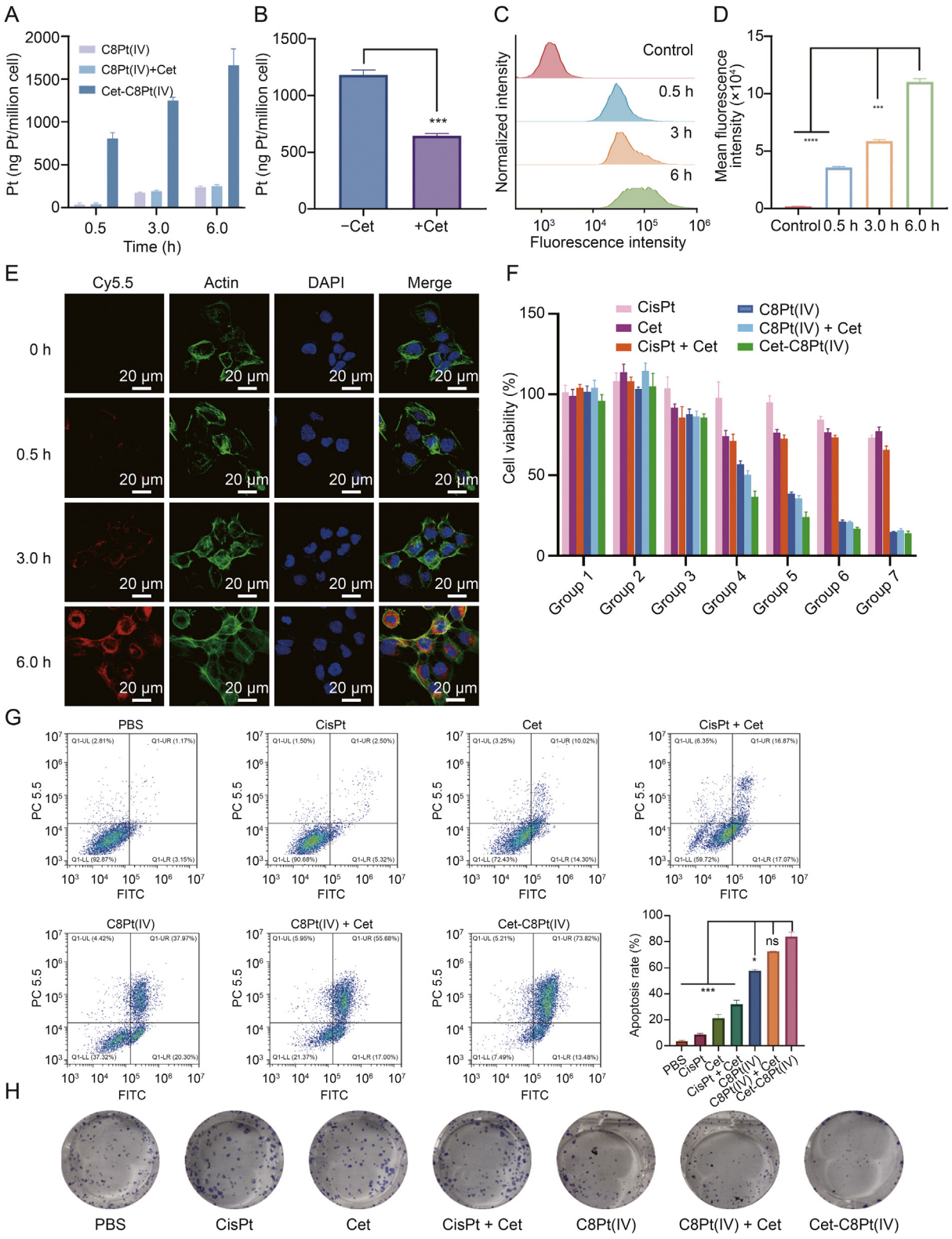

Fig. 3. Intracellular uptake, tumor targeting, and anti-tumor activity of cetuximab (Cet)-C8Pt(IV) *in vitro*. (A) Uptake of Cet-C8Pt(IV) by A-431 cells at different time points by inductively coupled plasma mass spectrometry (ICP-MS). (B) The platinum uptake by A-431 cells pre-treated with or without Cet by ICP-MS. (C, D) Flow cytometric curves (C) and the corresponding quantification (D) of the uptake of Cet-C8Pt(IV) by A-431 cells at different treatment durations. (E) The uptake of Cet-C8Pt(IV) by A-431 cells at different treatment durations by confocal laser scanning microscopy (CLSM). (F) Cell viability of A-431 treated with different drugs at 24 h by a 3-(4,5-dimethylthiazol-2-yl)-2,5-diphenyltetrazolium bromide (MTT) assay. Group 1: Pt, 0.000625 μM and Cet, 0.015 μg/mL; Group 2: Pt, 0.00625 μM and Cet, 0.15 μg/mL; Group 3: Pt, 0.0625 μM and Cet, 1.5 μg/mL; Group 4: Pt, 0.625 μM and Cet, 15 μg/mL; Group 5: Pt, 1.25 μM and Cet, 30 μg/mL; Group 6: Pt, 2.5 μM and Cet, 60 μg/mL; and Group 7: Pt, 5 μM and Cet, 120 μg/mL. (G) Apoptosis of A-431 cells treated with different drugs. (H) Colony formation of A-431 cells treated with various drugs after 14 days via a crystal violet staining assay. $^{*}P < 0.05$, $^{***}P < 0.001$, and $^{****}P < 0.0001$. DAPI: 4',6-diamidino-2-phenylindole; CisPt: cisplatin; PBS: phosphate-buffered saline; FITC: fluorescein isothiocyanate; UL: upper left; UR: upper right; LL: lower left; LR: lower right.

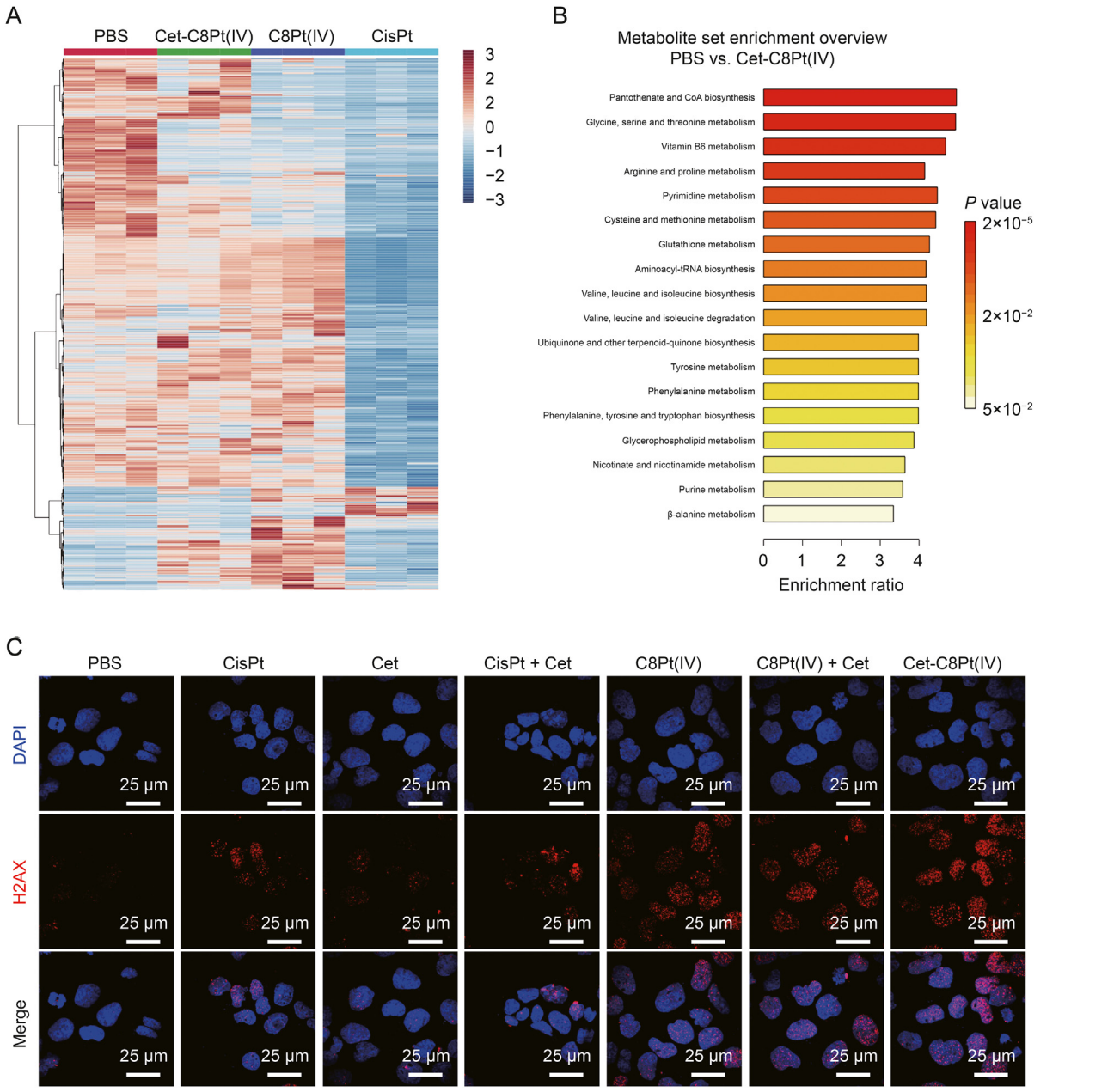

Fig. 4. Metabolomics analysis and DNA damage of A-431 cells treated with cetuximab (Cet)-C8Pt(IV). (A) A heat map showing the unsupervised hierarchical clustering of metabolites quantified by liquid chromatography/mass spectrometry (LC/MS). (B) Top 18 enriched Kyoto Encyclopedia of Genes and Genomes (KEGG) pathways. (C) DNA damage of cells with different treatments by confocal laser scanning microscope (CLSM) with γ-H2AX staining as a marker. PBS: phosphate-buffered saline; CisPt: cisplatin; tRNA: transfer RNA; DAPI: 4',6-diamidino-2-phenylindole.

Cet-C8Pt(IV) further exerted its anti-tumor effect by binding to EGFR, which is overexpressed in tumor cells. Therefore, effective tumor targeting can ensure sufficient drug efficacy. The tumor-targeting performance of Cet-C8Pt(IV) was verified *in vivo* using mouse models. First, the fluorescent dye Cy5.5 was used to label Cet and Cet-C8Pt(IV), resulting in Cet@Cy5.5 and Cet-C8Pt(IV)@Cy5.5, respectively. Subsequently, an orthotopic cSCC mouse model with high EGFR expression based on A-431 cells and a triple-negative breast cancer mouse model with low EGFR expression based on 4T1 cells were selected for subsequent studies. Fluorescence imaging using the IVIS small animal imaging system was used to monitor the distribution of Cet@Cy5.5 and Cet-C8Pt(IV)@Cy5.5 in mice after intravenous injection (Fig. 5A). The mice were euthanized 36 h after administration, and the biodistribution of Cet/Cet-C8Pt(IV) in the tumors and primary organs was examined. These findings indicated that the level of fluorescence intensity at the site of the tumor was notably greater in mice with A-431 tumors that received Cet treatment than in those with 4T1 tumors. Moreover, the fluorescence intensity was significantly higher at the tumor sites than in the heart, lungs, spleen, intestine, liver, and kidneys of mice bearing A-431 tumors treated with Cet-C8Pt(IV) and Cet (Fig. 5B). Additionally, at 3 h post-injection, strong fluorescence was observed at the tumor site of mice bearing A-431 tumors, with average fluorescence intensities of 1.206×10^9 p/s/cm^2/sr and 1.222×10^9 p/s/cm^2/sr. Nevertheless, the fluorescence in mice bearing 4T1 tumors was relatively weak (1.049×10^9 p/s/cm^2/

sr). In addition, the fluorescence in mice bearing A-431 tumors remained high and unchanged over time, whereas the opposite trend was observed in mice bearing 4T1 tumors (Fig. 5C). Lastly, the *ex vivo* imaging was used to quantify and analyze the average fluorescence in tumors and major organs. According to these findings, the mean fluorescence strength at the tumor site in mice carrying A-431 tumors receiving Cet treatment was only 1.7 times higher than that in mice receiving Cet-C8Pt(IV) treatment, whereas this was 3.1 times higher than that in mice bearing 4T1 tumors (Fig. 5D). Taken together, Cet-C8Pt(IV) targeted EGFR-overexpressing tumors in an orthotopic cSCC mouse model, accumulated rapidly, and was retained for a long time at tumor sites to exert its anti-tumor effect.

3.6. Anti-tumor ability of Cet-C8Pt(IV) in vivo

After exploring the biosafety and tumor targeting ability of Cet-C8Pt(IV), its anti-tumor effect was further studied in a mouse model bearing A-431 tumors. When the tumors reached approximately 100 mm^3, CisPt, Cet, CisPt + Cet, and Cet-C8Pt(IV) were administered via the tail vein at doses of 3 mg/kg of platinum and 10 mg/kg of Cet on days 0, 3, and 6 (Fig. 6A). On day 10 after the first treatment, the mice were euthanized and the tumor tissues were collected (Fig. 6B). From the first day of treatment (day 0) and every alternate day, the tumor volumes (Fig. 6C) and body weights (Fig. 6D) were recorded. During drug treatment, mice treated with CisPt or CisPt + Cet showed significant weight loss. The result showed that after the treatment, mice treated with CisPt lost approximately 18.6% of their initial starting body weight, whereas mice treated with CisPt + Cet lost approximately 18.9%. However, mice treated with Cet-C8Pt(IV) lost only approximately 8.6%, which was nearly equal to Cet. Moreover, mice treated with CisPt and CisPt + Cet developed marked scaling and hypothermia, whereas there were no apparent differences in skin, body temperature, or living conditions between those treated with Cet-C8Pt(IV) or PBS. These results demonstrate that Cet-C8Pt(IV) has a favorable safety profile.

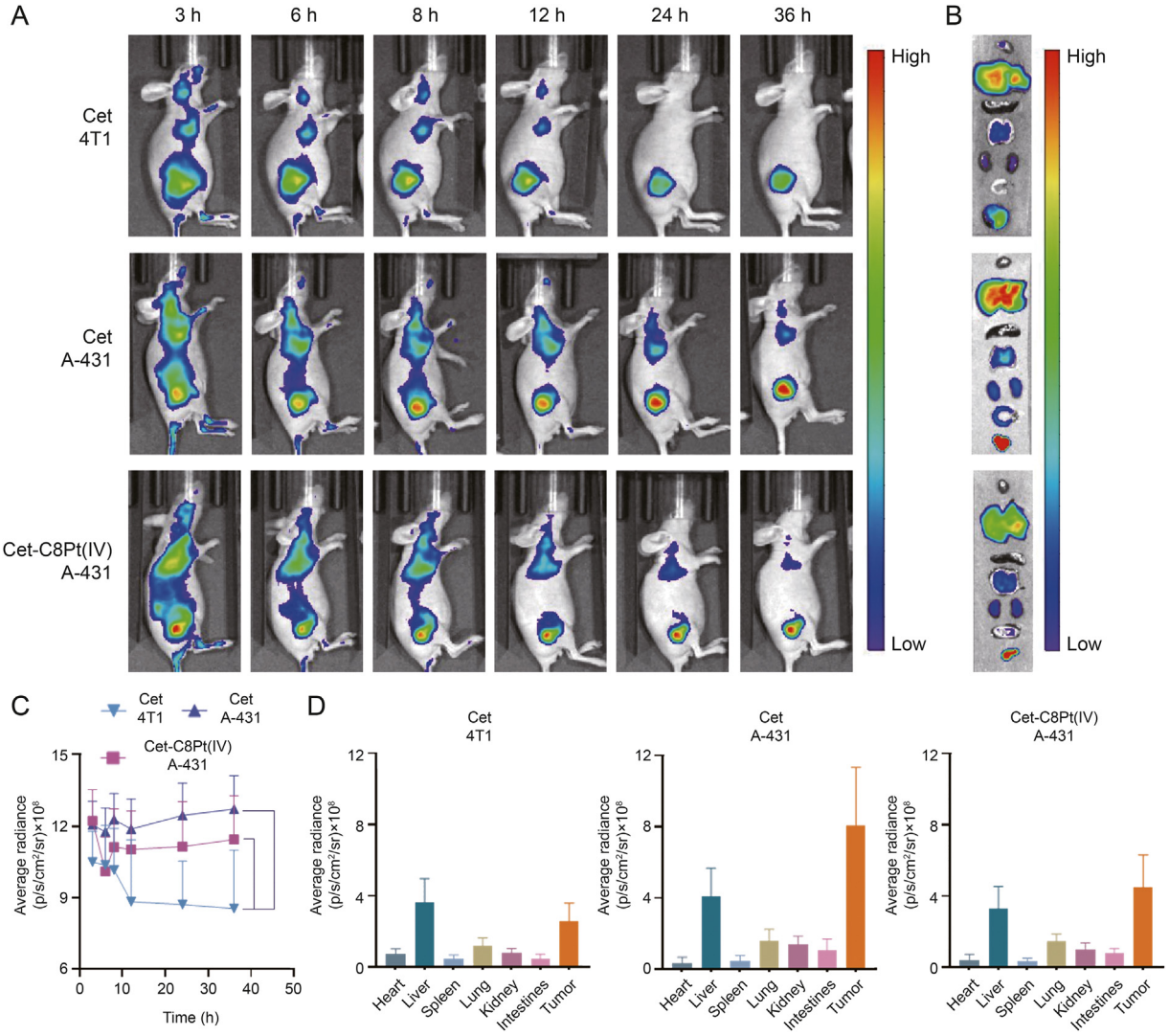

Fig. 5. The *in vivo* biodistribution of cetuximab (Cet)-C8Pt(IV) in mice models bearing A-431 and 4T1 tumors, respectively. (A) Biodistribution of Cet@Cy5.5 in mice bearing A-431 and 4T1 tumors and Cet-C8Pt(IV)@Cy5.5 in mice bearing A-431 tumors via fluorescence imaging at different time points. (B) *Ex vivo* imaging of tumors and major organs (top-down: heart, liver, spleen, lung, kidney, intestine, and tumor). (C) Quantification of fluorescence intensity in the tumors of mice bearing A-431 or 4T1 tumors at various time points. (D) The average fluorescence intensity of tumors and major organs of mice bearing A-431 and 4T1 tumors treated with Cet@Cy5.5 and Cet-C8Pt(IV)@Cy5.5 at 36 h post administration. $^{*}P < 0.05$ and $^{***}P < 0.001$.

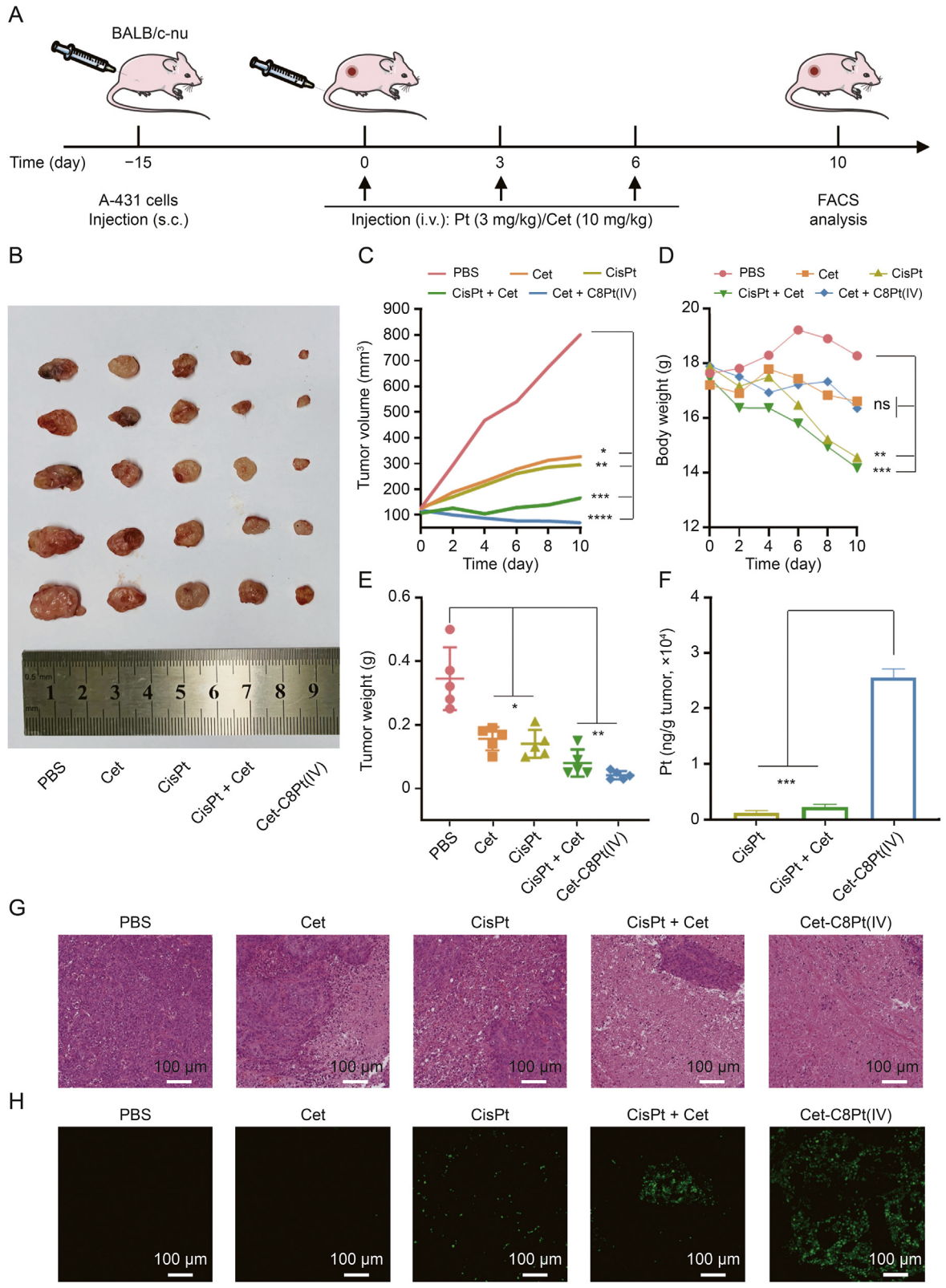

Fig. 6. The anti-tumor effect of cetuximab (Cet)-C8Pt(IV) on a mice model bearing A-431 tumors *in vivo*. (A) Schematic representation of the establishment of orthotopic cutaneous squamous cell carcinoma (cSCC) mouse model bearing A-431 tumors and the treatment process *in vivo*. (B) Digital images of tumors isolated from mice with various treatments at day 10 ($n = 5$). (C, D) Tumor growth curves (C) and body weights (D) of mice with various treatments. (E) *Ex vivo* tumor weight of mice with various treatments. (F) Platinum in tumors of mice with various treatments by inductively coupled plasma mass spectrometry (ICP-MS). (G, H) Hematoxylin and eosin (H&E) (G) staining and terminal deoxynucleotidyl transferase dUTP nick end labeling (TUNEL) (H) staining of tumor tissues of mice with different treatments. $^{*}P < 0.05$, $^{**}P < 0.01$, $^{***}P < 0.001$, and $^{****}P < 0.0001$. FACS: fluorescence-activated cell sorting; PBS: phosphate-buffered saline; CisPt: cisplatin.

After the mice were euthanized, the tumors were collected. The findings indicated a significant decrease in the average tumor weight of mice administered Cet-C8Pt(IV) (0.04 g) compared to those treated with PBS (0.344 g), CisPt (0.14 g), Cet (0.156 g), or CisPt + Cet (0.08 g) (Fig. 6E). Further characterization of the platinum drugs in the tumor tissues of mice administered CisPt, CisPt + Cet, or Cet-C8Pt(IV) was possible using ICP-MS. According to these findings, the platinum levels in the tumor tissues of mice that received Cet-C8Pt(IV) were 19.9 and 10.5 times greater compared to mice administered CisPt and CisPt + Cet, respectively (Fig. 6F). In addition, mice treated with CisPt and CisPt + Cet exhibited modest tumor shrinkage (tumor inhibition rates of approximately 59.3% and 76.7%). In contrast, mice treated with Cet-C8Pt(IV) demonstrated a notable suppressive effect on tumor growth (tumor inhibition rate of approximately 87.8%), confirming that the anti-tumor ability of Cet-C8Pt(IV) was significantly superior to that of CisPt and CisPt + Cet.

H&E and TUNEL staining further indicated that Cet-C8Pt(IV) had a robust therapeutic effect, as evidenced by extensive nuclear fragmentation and dissolution of tumor cells in mice treated with Cet-C8Pt(IV), surpassing the effects observed in mice treated with CisPt (Fig. 6G). Furthermore, TUNEL staining indicated a highly significant increase in green fluorescence intensity (representing DNA damage) in the tumor tissues of mice administered Cet-C8Pt(IV) compared to those administered CisPt (Fig. 6H). Taken together, Cet-C8Pt(IV) showed stronger anti-tumor activity *in vivo* than CisPt.

4. Conclusion

Monoclonal antibodies and potent cytotoxic drugs are combined in ADCs, which are considered as a promising group of anticancer agents with targeted properties and anti-tumor effects. Cet has limited anti-tumor effects in patients who are elderly and/or have advanced cSCC and who are unable to undergo surgery and combined chemotherapy; however, platinum drugs have considerable toxic side effects, and their effective doses may exceed the maximum tolerated dose in these patients. Hence, ADCs are considered as the preferred treatment option for tumors due to their excellent targeting ability, safety, and anti-tumor activity. However, the synthesis of the linkers of traditional ADCs is generally complicated, thereby resulting in high costs. In addition, the payloads of current ADCs have strong cytotoxic effects but with a relatively narrow therapeutic range. A novel ADC drug (Cet-C8Pt(IV)) was designed and developed using a platinum (IV) prodrug of CisPt, C8Pt(IV), as a payload with high cytotoxicity. Notably, the synthesis was concise and the conjugate was stable. In addition, payload C8Pt(IV) is broadly applicable to multiple tumor types and has a strong tumor-killing ability. Therefore, Cet-C8Pt(IV) enables the direct delivery of the potent cytotoxic payload, C8Pt(IV), directly to tumor cells, as Cet is bound with high affinity to EGFR overexpressed on cSCC cells. In the reductive tumor intracellular environment, C8Pt(IV) can be chemically reduced to CisPt with high toxicity, thereby increasing the antitumor activity efficiently with a synergistic anti-tumor effect. Furthermore, metabolomic analysis showed that Cet-C8Pt(IV) aggravated DNA damage in cSCC cells via the vitamin B6 metabolism pathway. In summary, Cet-C8Pt(IV) displayed a favorable safety profile and induced a robust anti-tumor effect.

CRediT author statement

Xiangye Yin: Conceptualization, Data curation, Formal analysis, Writing - Original draft preparation; **Yingjie Zhuang:** Formal analysis, Methodology, Writing - Original draft preparation; **Haiqin Song:** Resources, Funding acquisition, Supervision; **Yujian Xu:** Formal analysis; **Fan Zhang:** Methodology, Investigation; **Jianxin Cui:** Investigation, Formal analysis; **Lei Zhao:** Investigation; **Yingjie Yu:** Resources, Conceptualization; **Qixu Zhang:** Supervision, Conceptualization; **Jun Ye:** Resources, Supervision, Conceptualization; **Youbai Chen:** Conceptualization, Resources, Writing - Reviewing and Editing; **Yan Han:** Resources, Funding acquisition, Supervision, Conceptualization, Writing - Reviewing and Editing.

Declaration of competing interest

The authors declare that there are no conflicts of interest.

Acknowledgments

This work was supported by the National Natural Science Foundation of China (Grant No.: 51803120).

Appendix A. Supplementary data

Supplementary data to this article can be found online at https://doi.org/10.1016/j.jpha.2023.11.002.

References

[1] C.H. Chau, P.S. Steeg, W.D. Figg, Antibody-drug conjugates for cancer, Lancet 394 (2019) 793–804.
[2] P. Tarantino, R. Carmagnani Pestana, C. Corti, et al., Antibody-drug conjugates: Smart chemotherapy delivery across tumor histologies, CA Cancer J. Clin. 72 (2022) 165–182.
[3] A. Thomas, B.A. Teicher, R. Hassan, Antibody-drug conjugates for cancer therapy, Lancet Oncol. 17 (2016) e254–e262.
[4] R.S. Schwartz, Paul Ehrlich's magic bullets, N. Engl. J. Med. 350 (2004) 1079–1080.
[5] J.Z. Drago, S. Modi, S. Chandarlapaty, Unlocking the potential of antibody-drug conjugates for cancer therapy, Nat. Rev. Clin. Oncol. 18 (2021) 327–344.
[6] C.M. Yamazaki, A. Yamaguchi, Y. Anami, et al., Antibody-drug conjugates with dual payloads for combating breast tumor heterogeneity and drug resistance, Nat. Commun. 12 (2021), 3528.
[7] K. Tsuchikama, Z. An, Antibody-drug conjugates: Recent advances in conjugation and linker chemistries, Protein Cell 9 (2018) 33–46.
[8] J.D. Bargh, A. Isidro-Llobet, J.S. Parker, et al., Cleavable linkers in antibody-drug conjugates, Chem. Soc. Rev. 48 (2019) 4361–4374.
[9] E. Merkul, N.J. Sijbrandi, J.A. Muns, et al., First platinum(II)-based metal-organic linker technology (Lx®) for a plug-and-play development of antibody-drug conjugates (ADCs), Expert Opin. Drug Deliv. 16 (2019) 783–793.
[10] A. Pryyma, S. Gunasekera, J. Lewin, et al., Rapid, high-yielding solid-phase synthesis of cathepsin-B cleavable linkers for targeted cancer therapeutics, Bioconjug. Chem. 31 (2020) 2685–2690.
[11] J.T.W. Tong, P.W.R. Harris, M.A. Brimble, et al., An insight into FDA approved antibody-drug conjugates for cancer therapy, Molecules 26 (2021), 5847.
[12] P.J. Kennedy, C. Oliveira, P.L. Granja, et al., Antibodies and associates: Partners in targeted drug delivery, Pharmacol. Ther. 177 (2017) 129–145.
[13] T. Wu, M. Liu, H. Huang, et al., Clustered nanobody-drug conjugates for targeted cancer therapy, Chem. Commun. 56 (2020) 9344–9347.
[14] L. Zhang, Y. Wang, J. Karges, et al., Tetrahedral DNA nanostructure with interferon stimulatory DNA delivers highly potent toxins and activates the cGAS-STING pathway for robust chemotherapy and immunotherapy, Adv. Mater. 35 (2023), 2210267.
[15] M.L. Gillison, A.M. Trotti, J. Harris, et al., Radiotherapy plus cetuximab or cisplatin in human papillomavirus-positive oropharyngeal cancer (NRG Oncology RTOG 1016): A randomised, multicentre, non-inferiority trial, Lancet 393 (2019) 40–50.
[16] A. Picard, F. Pedeutour, F. Peyrade, et al., Association of oncogenic mutations in patients with advanced cutaneous squamous cell carcinomas treated with cetuximab, JAMA Dermatol. 153 (2017) 291–298.
[17] Q. Jin, S. Yan, H. Hu, et al., Enhanced chemodynamic therapy and chemotherapy via delivery of a dual threat ArtePt and iodo-click reaction mediated glutathione consumption, Small Meth. 5 (2021), 2101047.
[18] H. Xiao, R. Qi, S. Liu, et al., Biodegradable polymer – cisplatin(IV) conjugate as a pro-drug of cisplatin(II), Biomaterials 32 (2011) 7732–7739.
[19] X. Kang, Y. Wang, Z. Chen, et al., Imidazole modified Pt(iv) prodrug-loaded multi-stage pH responsive nanoparticles to overcome cisplatin resistance, Chem. Commun. 56 (2020) 11271–11274.
[20] M. Ravera, E. Gabano, M.J. McGlinchey, et al., Pt(IV) antitumor prodrugs: Dogmas, paradigms, and realities, Dalton Trans. 51 (2022) 2121–2134.

[21] H. Huang, Y. Dong, Y. Zhang, et al., GSH-sensitive Pt(IV) prodrug-loaded phase-transitional nanoparticles with a hybrid lipid-polymer shell for precise theranostics against ovarian cancer, Theranostics 9 (2019) 1047–1065.
[22] X. Ling, X. Chen, I.A. Riddell, et al., Glutathione-scavenging poly(disulfide amide) nanoparticles for the effective delivery of Pt(IV) prodrugs and reversal of cisplatin resistance, Nano Lett. 18 (2018) 4618–4625.
[23] L. Zhang, K. Shang, X. Li, et al., Reduction sensitive polymers delivering cationic platinum drugs as STING agonists for enhanced chemo-immunotherapy, Adv. Funct. Mater. 32 (2022), 2204589.
[24] E. Wexselblatt, D. Gibson, What do we know about the reduction of Pt(IV) pro-drugs? J. Inorg. Biochem. 117 (2012) 220–229.
[25] D. Gibson, Platinum(IV) anticancer prodrugs - hypotheses and facts, Dalton Trans. 45 (2016) 12983–12991.
[26] Y. Yu, L. Zhang, Z. Qin, et al., Unraveling and overcoming platinum drug-resistant cancer tumors with DNA nanostructures, Adv. Funct. Mater. 33 (2023), 2208797.
[27] G. Xiong, D. Huang, L. Lu, et al., Near-infrared-II light induced mild hyperthermia activate cisplatin-artemisinin nanoparticle for enhanced chemo/chemodynamic therapy and immunotherapy, Small Meth. 6 (2022), 2200379.
[28] N. Heemskerk, M. Gruijs, A.R. Temming, et al., Augmented antibody-based anticancer therapeutics boost neutrophil cytotoxicity, J. Clin. Invest. 131 (2021), 134680.
[29] D.E. Gerber, H. Choy, Cetuximab in combination therapy: From bench to clinic, Cancer Metastasis Rev. 29 (2010) 171–180.
[30] A. Stratigos, C. Garbe, C. Lebbe, et al., Diagnosis and treatment of invasive squamous cell carcinoma of the skin: European consensus-based interdisciplinary guideline, Eur. J. Cancer 51 (2015) 1989–2007.
[31] S.K.T. Que, F.O. Zwald, C.D. Schmults, Cutaneous squamous cell carcinoma: Management of advanced and high-stage tumors, J. Am. Acad. Dermatol. 78 (2018) 249–261.
[32] S.K.T. Que, F.O. Zwald, C.D. Schmults, Cutaneous squamous cell carcinoma: Incidence, risk factors, diagnosis, and staging, J. Am. Acad. Dermatol. 78 (2018) 237–247.
[33] T. Tedeschini, B. Campara, A. Grigoletto, et al., Polyethylene glycol-based linkers as hydrophilicity reservoir for antibody-drug conjugates, J. Control. Release 337 (2021) 431–447.
[34] Z. Ma, M. Kang, S. Meng, et al., Selective killing of Shiga toxin-producing *Escherichia coli* with antibody-conjugated chitosan nanoparticles in the gastrointestinal tract, ACS Appl. Mater. Interfaces 12 (2020) 18332–18341.
[35] W.-H. Chen, Q.-W. Chen, Q. Chen, et al., Biomedical polymers: Synthesis, properties, and applications, Sci. China Chem. 65 (2022) 1010–1075.
[36] L. Galluzzi, I. Vitale, L. Senovilla, et al., Prognostic impact of vitamin B6 metabolism in lung cancer, Cell Rep. 2 (2012) 257–269.
[37] K. Fatima, N. Masood, Z. Ahmad Wani, et al., Neomenthol prevents the proliferation of skin cancer cells by restraining tubulin polymerization and hyaluronidase activity, J. Adv. Res. 34 (2021) 93–107.
[38] T.K. Nayak, C.A.S. Regino, K.J. Wong, et al., PET imaging of HER1-expressing xenografts in mice with ^{86}Y-CHX-A''-DTPA-cetuximab, Eur. J. Nucl. Med. Mol. Imag. 37 (2010) 1368–1376.
[39] A.M. Sochaj, K.W. Świderska, J. Otlewski, Current methods for the synthesis of homogeneous antibody-drug conjugates, Biotechnol. Adv. 33 (2015) 775–784.
[40] M.J. Birrer, K.N. Moore, I. Betella, et al., Antibody-drug conjugate-based therapeutics: State of the science, J. Natl. Cancer Inst. 111 (2019) 538–549.
[41] Z. Dai, X. Zhang, Q. Cheng, et al., Site-specific antibody-drug conjugates with variable drug-to-antibody-ratios for AML therapy, J. Control. Release 336 (2021) 433–442.
[42] C. Yu, C. Yang, X. Song, et al., Long non-coding RNA expression profile in broiler liver with cadmium-induced oxidative damage, Biol. Trace Elem. Res. 199 (2021) 3053–3061.
[43] X. Huo, K.B. Dunbar, X. Zhang, et al., In Barrett's epithelial cells, weakly acidic bile salt solutions cause oxidative DNA damage with response and repair mediated by p38, Am. J. Physiol. Gastrointest. Liver Physiol. 318 (2020) G464–G478.
[44] X. Feng, L. Ma, J. Lei, et al., Piezo-augmented sonosensitizer with strong ultrasound-propelling ability for efficient treatment of osteomyelitis, ACS Nano 16 (2022) 2546–2557.
[45] H. Xiao, R. Qi, T. Li, et al., Maximizing synergistic activity when combining RNAi and platinum-based anticancer agents, J. Am. Chem. Soc. 139 (2017) 3033–3044.
[46] S. O'Grady, S.P. Finn, S. Cuffe, et al., The role of DNA repair pathways in cisplatin resistant lung cancer, Cancer Treat. Rev. 40 (2014) 1161–1170.
[47] Y. Wang, Y. Jiang, D. Wei, et al., Nanoparticle-mediated convection-enhanced delivery of a DNA intercalator to gliomas circumvents temozolomide resistance, Nat. Biomed. Eng. 5 (2021) 1048–1058.
[48] J. Ding, H. Xiao, X. Chen, Advanced biosafety materials for prevention and theranostics of biosafety issues, Biosaf. Health 4 (2022) 59–60.
[49] Y. Zhang, Z. Li, J. Milon Essola, et al., Biosafety materials: Ushering in a new era of infectious disease diagnosis and treatment with the CRISPR/Cas system, Biosaf. Health 4 (2022) 70–78.
[50] A. Beck, L. Goetsch, C. Dumontet, et al., Strategies and challenges for the next generation of antibody-drug conjugates, Nat. Rev. Drug Discov. 16 (2017) 315–337.